Journal of Manufacturing Engineering, September 2022, Vol. 17, Issue. 3, pp 104-110

STRUCTURAL AND THERMAL PROPERTIES OF A SELECTED HOST CRYSTAL LATTICE: EXPLORATION OF INHERENT POSSIBILITIES

Sanjay Kumar Dubey[1] and *Shashank Sharma[2]

[1]Department of Physics, Dr Radha Bai, Govt. Navin Girls College, Raipur, Chhattisgarh- 492001, India
[2]Department of Physics, Govt. ERR PG Science College, Bilaspur, Chhattisgarh- 495006, India

ABSTRACT

Host $Ba_2MgSi_2O_7$ phosphor was successfully prepared via a low-temperature combustion synthesis route. The phase identification of the prepared phosphor was made with the help of the powder XRD technique. The XRD pattern of the phosphor revealed its monoclinic crystal symmetry with a space group C2/c. The XRD pattern has been well clarified with JCPDS PDF card no. #23-0842. The average crystallite size was calculated as 42nm, and the crystal lattice strain size was calculated as 0.24, respectively. It is acquired that the sample UV exposed for 15min gives optimum TL intensity at 112.19^0C temperature and displays a single TL glow peak. Based on TL glow curve, it can be suggested that the $Ba_2MgSi_2O_7$ (BMS) phosphor is an efficient host lattice but not a better TL phosphor. In our present study, we have discussed the XRD, FESEM and thermo-luminescence (TL) characteristics and different kinetic parameters of this phosphor.

Keywords: *X-ray Diffraction Pattern (XRD), $Ba_2MgSi_2O_7$ (BMS), Monoclinic, C2/c and Combustion Synthesis*

1. Introduction

Since the 21st century, national progress has been closely linked with scientifically and technologically developed, and that linkage has intensified in the last few decades. The nano materialistic research achievement is more important and necessary in the progressive development of the technological era. Our new innovative rare earth do-pant ions such as Eu, Er, Tb, Dy and Ce are more essential parts of our advanced materialistic achievements of optical display system lightening LEDs. But the biggest challenge is finding a worthy host crystal lattice. Green nature-inspired manufacturing technologies for sustainable development are the key issues that environmental biomaterial addresses. Thermo Kinetic parameters are an essential analytic part that many applications in nanomaterials and high-temperature dosimetry radiation. It is concerned with a thermal stimulation process that can be initiated by changing temperature. Emerging technologies and nano applications demand advanced, innovative high-tech materials like silicates, aluminates and sulfides approach investigated highly. Biomaterials are living organisms bioactive molecules in vitro and vivo used in tissue engineering [1]. Various characterization methods for all prepared samples were utilized to briefly investigate the phase structure, average particle size and surface morphology. Inorganic solid-state silicates have become a focus of technological interest due to their favourable physical and chemical properties.

For various applications, various silicate host materials doped with rare-earth and other ions have been widely investigated as luminescent materials. The best long persistent phosphor known till now is $SrAl_2O_4$: Eu^{2+}, $Dy^{3+,}$ which is a commercial phosphor and may have afterglow for more than 20 hours [2,3]. Many of the silicate-based phosphors doped with divalent or trivalent rare-earth ions, likewise Eu^{2+}, Dy^{3+}, Ce^{3+}, Er^{3+} have been preferred for use as commercial phosphor in fluorescent lamps, scintillators [4,5], plasma display panels, white light emitting diodes (WLEDs), long persistent phosphor, high-temperature radiation dosimetry applications. In monoclinic $Ba_2MgSi_2O_7$, crystal structures have been displayed at octahedral [BaO_8] sites because of the octahedral coordination number of Ba^{2+} ion and tetrahedral for both Mg^{2+} and Si^{4+} ions [6]. Dubey et al. proposed that the $Ba_2MgSi_2O_7$ has revealed a monoclinic structure with space group C2/c [7]. Our only intention behind this present research investigation is to find out the possibility of better performance in a suitable host crystal lattice, as the selection of a better host material drives the entrepreneurship of the main characteristics (such as structural and thermal) of any phosphor. In this paper, the host $Ba_2MgSi_2O_7$ sample was successfully

*Corresponding Author - E- mail: dr.shashankeinstein@rediffmail.com

synthesized via the combustion synthesis technique, and its structural properties, such as XRD, and FESEM and thermal characteristics, such as thermoluminescence (TL) spectra, have also been briefly discussed.

2. Experimental Section

2.1 Sample Synthesization Process

Melilite compounds are a very large group family of compounds, which are depicted with a general structural composition representation such as $M_2X^1Y^2{}_2O_7$, [where M; denotes Ba, Sr & Ca, X^1; denotes Mg, Zn, Cu, Mn & Co and Y^2; denotes Ge & Si]. Melilites are broadly studied as optical materials [8]. Low-temperature combustion synthesis route is one of the best synthesization routes as compared to other synthesis techniques. In this technique, very low heating temperatures and less time for phosphor synthesization are required. We applied in our experiment; $Ba_2MgSi_2O_7$ (BMS) were successfully synthesized via a low-temperature combustion synthesis route. As an initial raw chemical, for the preparation of pure $Ba_2MgSi_2O_7$ sample, $Ba(NO_3)_2$ Mg $(NO_3)_2$, $SiO_2{*}H_2O$, NH_2CONH_2 (Urea) and H_3BO_3 were used in our experiment, including with AR grade (99.99% purity). The precursor chemicals were taken according to their respective stoichiometric ratio required to prepare the desired phosphor and mixed in a mortar pestle. Urea (NH_2CONH_2) has been used as a combustion fuel, and boric acid (H_3BO_3) has also been employed as an oxidizer or flux. The stoichiometric ratio of the precursor powders with acetone (CH3COCH3) was grinded thoroughly in an agate mortar pestle for 2 hours before being transferred to a cylindrical silica crucible. Then the mixture was fired at 650^{o}C in a muffle furnace. The mixture undergoes thermal dehydration and ignites at 1000^{0}C for 1h with the liberation of gaseous products to yield silicates. The entire combustion process was completed in about 5min. The products obtained by combustion were fluffy masses and converted into fine powder after additional crushing. The resulting sample was restored in an airtight bottle for structural and optical characterization studies [10]. The sintered BMS sample was obtained as an optically translucent (i.e. semi-transparent) and white (i.e. colorless) powder.

The chemical reaction of this process is given as follows:

$$Ca(NO_3)_2 + Mg(NO_3)_2 + SiO_2{*}H_2O + NH_2CONH_2 + H_3BO_3 \rightarrow Ca_2MgSi_2O_7 + H_2O(\uparrow) + CO_2(\uparrow) + N_2(\uparrow) \quad (1)$$

For the combustion process of oxides, metal nitrates are applied as oxidizers and urea is also applied as a reducer [9]. With the calculation of oxidizer to fuel ratio, the elements were assigned formal valences as follows: Ba = +2, Mg = +2, Si = +4, B = +3, C = +4, H = +1, O= -2 and N = 0. Thus, the heat of combustion is maximum for Oxidizer/Fuel ratio is equal to 1 [10].

2.2 Sample Characterization

XRD of the crystalline structure, size and phase composition of the synthesized phosphor was noted with the help of Bruker D8 advance X-ray diffractometer with Cu-K_α radiation having wavelength (λ = 1.5405Å), at 40 kV, and 40 mA voltage and current values, respectively. The surface morphology of the sample was examined with the help of FESEM (ZEISS model microscope). A routine Thermo-luminescence (TL) study of the UV-irradiated (254 nm) samples was recorded with the help of routine TL set-up Nucleonix TL 1009I TLD reader (Integral-PC Based) with constant heating rate 5^0Cs^{-1}. All experiments were performed in identical conditions, and it was observed that the results were reproducible. All data was carried out at room temperature.

3. Results and Discussion

3.1 XRD Analysis

XRD patterns were recorded in the range between (10^0\2θ\$80^0$) of un-doped $Ba_2MgSi_2O_7$ powder sample was successfully synthesized by combustion synthesis route. All the peaks have been displayed in Fig. 1, according to the standard JCPDS PDF file No. 23-0842 [11]. The cell volume and the following lattice parameters were also examined [12]. All parameters are shown in Table no. 1. We have suggested that the prepared sample is better than the host material.

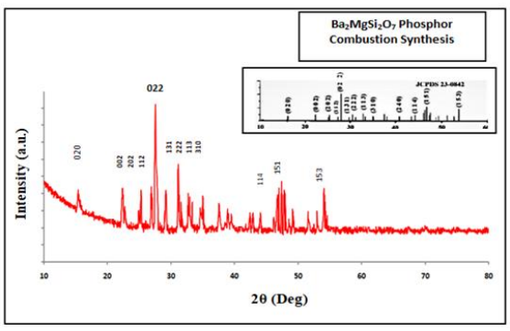

Fig. 1 XRD Pattern of Synthesized BMS Phosphor

A few extra peaks were displayed in the XRD patterns. XRD diffraction peaks were peaked at (15.35), (22.42), (25.25), (26.88), (27.51), (29.22), (31.16), (32.69), (34.92), (44.14), (47.39), and (54.14) corresponding to (020), (002), (202), (112), (022), (131), (222), (113), (310), (114), (151), and (153) planes respectively and Sharper and isolated XRD peaks likewise 2θ = 22.42 (002), 27.51 (022), 29.22 (131), 31.16 (222), 32.69 (113), 54.14 (153) were selected for crystallite size estimation. The XRD pattern confirms that the pure phase of monoclinic $Ba_2MgSi_2O_7$ formed at an annealing temperature of 1000^0C for 1h.

3.1.1 Debay-Scherrer formula

Debye–Scherrer empirical formula is represented as follows to determine the crystallite size (D),

$$D = k\lambda/ \beta Cos\theta \quad (2)$$

Where k = 0.94 (Scherrer constant), λ is the wavelength of occurrence X-ray (for Cu-K_α radiation, λ = 1.5406Å), β is the FWHM (Full width half maximum) of the peaks and θ (theta) is presented the corresponding Braggs diffraction angle [13], as well as D, denotes crystallite size. The lattice parameters of sintered phosphor materials have shown in Table1.

Table 1 Lattice Parameters of BMS Phosphor

No.	Lattice Parameters	Properties
1.	Crystal Structure	Monoclinic
2.	Space Group	C2/c
3.	Lattice Parameters	a = 8.4128 Å, b=10.7101 Å, c = 8.4387 Å & $\alpha=90^0$, $\beta=110.71°$ $\gamma=90^0$
4.	Cell Volume	711 $(Å)^3$
5.	Radiation	Cu-K_α
6.	Incident X-ray Wavelength	1.5406 Å

3.1.2 Williamson-Hall (W-H) Plot Method of Analysis

This method is based on Uniform Deformation Model (UDM). Using this method, we obtain the graph between βCosθ and 4Sinθ. Fig. 3 displays the W-H plot of the various diffraction peaks of BMS phosphor. The Williamson-Hall (W-H) method is one of the best methods to consider the effect of strain-induced X-ray diffraction [XRD] peak extension. In addition, this method provides the calculation of the intrinsic strain as well as crystalline size [14,15].

This method is seen as very important and useful from the point of view of estimating the crystal lattice strain present in the synthesized samples. In this way, FWHM can be represented as a linear combination of the major role of the crystallite size & crystal lattice strain [16]. The crystal lattice strain induced broadening in the powder material was calculated via the following mathematical relation given below:

$$\beta Cos\theta = k\lambda/D + 4\varepsilon Sin\theta \quad (3)$$

Where, 'β= 2 (θ_2-θ_1)'; indicates the FWHM (in radians), 'θ' indicates the Bragg angle of the peak, 'λ' (i.e. 1.5406 Å); indicates the wavelength of X-ray used, 'D'; indicates the effective particle size and 'ε'; indicates the effective crystal lattice strain [17].

Table 2 Determination of Average Crystallite Size and Lattice Strain Size

Diffraction Angle	Respective Plane	Debye Scherer's (nm)	W-H Plots (nm)	Strain (nm)
22.42	002	40	56	0.23
27.57	022	48	60	0.24
29.22	131	42	52	0.25
31.16	222	46	58	0.24
32.69	113	44	56	0.24
54.14	153	44	54	0.25
Average Size		~44nm	~56nm	0.24

The determination of the effective particle size [D] for which the crystal lattice strain is taken into account can be extrapolated from the plot, as clearly displayed in Fig. 2.

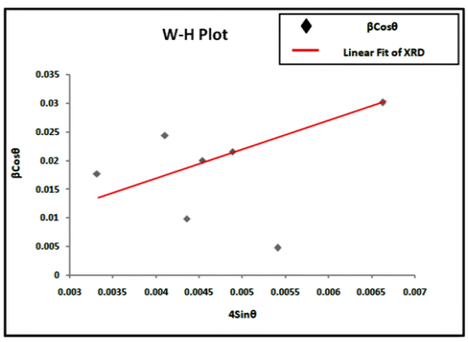

Fig. 2 Williamson-Hall Plot of $Ba_2MgSi_2O_7$ Phosphor

The crystal lattice strain was determined from the slope, and the crystalline size was determined from the y-intercept of the linear fit. The W-H plots demonstrate that the line extension was essentially isotropic, which indicates that the diffraction domains were isotropic and present with a small percentage of microscopic strain. Sharper and isolated XRD peaks likewise 2θ = 22.42 (002), 27.51 (022), 29.22 (131), 31.16 (222), 32.69 (113), 54.14 (153) were selected for crystallite size and crystal lattice strain determination. The average crystallite size was calculated as 44nm with the help of Debye Scherer's mathematical formula and 56nm using the Williamson–Hall (W–H) plot method. The average crystal size and average crystal lattice strain size (Table 2) of the synthesized sample were obtained to be the maximum value calculated by the W-H plot method as compared to the Debye scherrer method.

3.2 FESEM Analysis

In Fig. 3 (a), the surface morphology of the prepared phosphor is displayed with different magnifications. A closer examination of the FESEM image demonstrates that the particle's surface morphology was not uniform. At the same time, they were very tightly clustered to form numerous secondary particles [18].

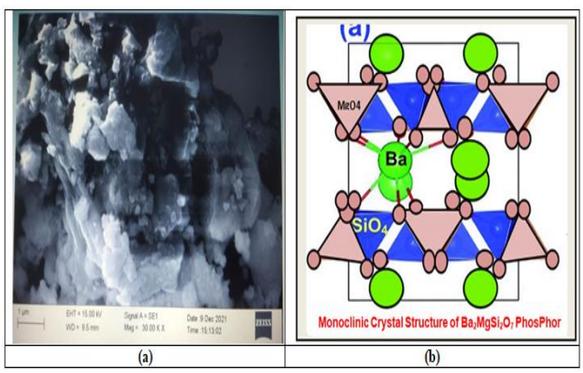

Fig. 3 (a) FESEM Image and (b) Crystal Structure

One FESEM image represents that all samples have smooth and homogeneous crystal structures with isolated pores. From the FESEM image, it can be examined that the particles with different size distributions are present in the prepared sample. Furthermore, these samples have been prepared by low-temperature heat treatment, due to which some large aggregates exist.

3.3 TL Spectra Analysis

Thermo-luminescence phosphor display afterglow characteristics, known as persistent luminescence. They are very needful in various applications, brightness in the dark road, bio-imaging and emergency signs. At present, the evolution of novel TL materials demonstrates a new and rapidly developing application of research in physics, medicine, mineral prospering, archaeological dating, forensic science and high-temperature radiation dosimetry [19].

Fig. 4 displays that the single TL glow curve of prepared $Ba_2MgSi_2O_7$ phosphor has been obtained with 15min UV irradiation time at a constant heating rate of 5^oCs^{-1}. For TL measurement, a fixed amount of the powder specimens were kept (8mg) in the cavity. The TL glow curve peak was allocated at 112.41^{o}C temperature, respectively, and these peak positions remain constant with UV irradiation time. In our case, the TL peak is very weak and can be neglected. Observing the TL glow curve, we find that the maximum glow curve is obtained at 112.41^{o}C. From 68.45^{o}C temperature, TL intensity is continuously increasing up to 112.41^{o}C. After that, the TL intensity decreases continuously up to 168.37^{o}C temperature and near about flate and constant having the lowest value of TL intensity up to 300^{o}C temperature.

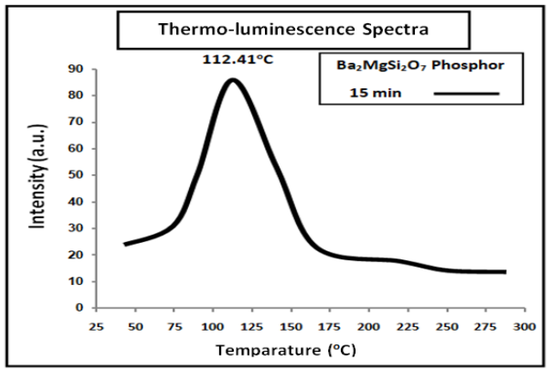

Fig. 4 TL Glow Curve of Pure $Ba_2MgSi_2O_7$ Phosphor with 15 min UV irradiation Time

The TL glow curve shows that, initially, thermo-luminescence [TL] intensity increases with increasing UV irradiation time. The optimum TL intensity is maximum for 15 min of UV exposure; after that, they start to decrease. It is predicted that with the increasing UV irradiation time, a large amount of charge carriers are released, which increases the trap density and results in an increase of TL intensity (density of

charge carrier may have been increasing), but after a specific exposure (15 min) traps density starts to destroy results in decrease in TL intensity [20].

3.3.1 Calculation of Kinetic Parameters

The thermo-luminescence (TL) characteristics of phosphors mainly depend on the kinetic parameters i.e., Trap-depth or activation energy (E), order of kinetics (b), and the frequency factor (s) describing the trapping emitting centers which is quantitatively responsible for the thermo-luminescence (TL) emission. TL phosphors exhibit glow curves with one or more peaks when the charge carriers are released. There are various methods for determining the kinetic parameters from TL glow curves. For example, when one of the TL glow peaks is highly isolated from the others, the experimental technique, such as the peak shape method, is appropriate to determine kinetic parameters. The TL parameters for the prominent glow peak of sintered phosphor were calculated with the help of the peak shape method [21,22].

[a] Order of Kinetics (b)

It depends on the peak shape of TL glow curve. The mechanism of recombining de-trapped charge carriers with their counterparts is called the order of kinetics [b]. The kinetic order for the glow peak of $Ba_2MgSi_2O_7$ phosphor can be determined via calculating the geometrical factor μ_g from the mathematical relation as follows:

$$\mu_g = {}^{\delta}/\omega = T_2\text{-}T_m/T_2\text{-}T_1 \quad (4)$$

Where T_m is the optimum peak temperature, T_1 and T_2 are temperatures at the half intensity on the ascending and descending parts of the glow peak, respectively, [$\omega = T_2 - T_1$], the high-temperature half width [$\delta = T_2 - T_m$]. The geometric factor differentiates between first and second-order TL glow peaks. [μ_g = 0.39-0.42] for the first order kinetics; [μ_g = 0.49-0.52] for the second order kinetics and [μ_g = 0.43-0.48] for the mixed order kinetics [23].

[b] Activation energy (E)

The activation energy [E] or trap depth can be determined by the general formula, which is valid for any kinetics. It is given by mathematical relation as follows:

$$E = C_\alpha (kT_m^2/\alpha) - b_\alpha (2kT_m) \quad (5)$$

For general order kinetics, the values of the C_α and b_α ($\alpha = \tau, \delta, \omega$) are expressed as $c_\tau = [1.51 + 3(\mu_g - 4.2)]$, $b_\tau = [1.58 + 0.42((\mu_g - 0.42)]$; $c_\delta = [0.976 + 7.3(\mu_g - 0.42)]$, $b_\delta = 0$ and $c_\omega = [2.52 + 10.2(\mu_g - 0.42)]$, $b_\omega = 1.0$.

[c] Frequency Factor (s^{-1})

It reflects the probability of electron escape from the traps after exposure to ionizing radiation. The frequency factor is one of the most significant parameters for material characterization. After obtaining the order of kinetics [b] and activation energy [E], the frequency factor [s] can be determined with the help of the following mathematical relation by replacing the values of E and b [23,24]:

$$\beta E/kT^2_m = s\,[1+ (b\text{-}1)\, 2kT_m /E] \exp(-E/kT_m) \quad (6)$$

Where k is the Boltzmann constant, E is the activation energy, b is an order of kinetics, T_m is the temperature of peak position, and β is the heating rate. In the present work, $\beta = 5^0 Cs^{-1}$.

The kinetic parameters were evaluated with the help of the thermo-luminescence (TL) glow curve of the prepared pure powder sample with different UV irradiation times at a constant heating rate $5^0 Cs^{-1}$ has been displayed and summarized in Table 3.

Table 3 The Kinetic Parameters for UV Irradiated $Ba_2MgSi_2O_7$ Phosphor

UV (in min)	T_m (^{o}C)	μ_g	E (eV)	(S^{-1})
15	112.41	0.47	56	7.8×10^7 s^{-1}

For pure $Ba_2MgSi_2O_7$ phosphor, the geometric shape factor (μ_g) is calculated to be 0.47. The corresponding Activation energy (E) and frequency factor (s^{-1}) were evaluated as 0.57eV and 7.8×10^7 s^{-1} respectively. In our experiments, the shape factor (μ_g) is a lie between (0.43-0.48), which indicates that it is a case of mixed order kinetics. In our case, this phosphor's thermo-luminescence [TL] peak is very weak because on heating the sample, the charge carriers leave their valance band, move towards the conduction band, and thus return straight back without falling into any trap there. The result is that the TL intensity is not that high. For this reason, we need doping of a suitable do-pant rare earth ion in the host crystal lattice site for trap construction. Because the do-pant ions generate a trap in the host crystal lattice site, the charge carriers get trapped there; that is, the charge carriers trapped in the

trap take more time to return, due to which their TL intensity increases.

4. Conclusion

In summary, Un-doped $Ba_2MgSi_2O_7$ (BMS) phosphor sample was successfully synthesized via a low-temperature combustion synthesis route, and its XRD, FESEM and Thermo-luminescence (TL) characteristics were briefly discussed in our experiment. The analysis of XRD patterns revealed that the single-phase monoclinic crystal structure of synthesized phosphor was confirmed. The synthesized sample's average crystal size and average crystal lattice strain size were obtained as the maximum value calculated by the W-H plot method compared to the Debye scherrer method. The grain size of the sintered phosphor in the nano range and homogeneity is much better. Based on a comparison of TL results, we can say that the host BMS phosphor has been shown thermal spectra at comparatively very low TL intensities. After this comprehensive study, it would be fair to say that the TL intensities do not achieve their optimal level due to the large band gap in the host materials. This is why the doping process should be adopted to narrow the gap so that TL glow curves can be obtained at higher intensities.

Acknowledgements

We gratefully acknowledge the kind support for the XRD and FTIR analysis facility, NIT Raipur (C.G.). The authors are also thankful to Pt. Ravishankar Shukla University, Raipur (C.G.), for providing the facility of thermoluminescence analysis. We are also heartily grateful to Dept. of physics, Dr. Radha Bai, Govt. Navin Girls College Mathpara Raipur (C.G.), providing the facility of muffle furnace and other essential research instruments.

Nomenclature

Symbol	Meaning	Unit
λ	Wavelength	Å
E	Activation Energy	eV
β	Heating Rate	$^0Cs^{-1}$
T	Temperature	$^0C/K$

References

1. *Bhatkar, V. B., & Bhatkar, N. V. (2011), Combustion synthesis and photoluminescence study of silicate biomaterials. Bulletin of Materials Science, Vol. 34: 1281-1284.*
2. *Garlick, G.F.J.; Gibson, A.F. (1948), The electron trap mechanism of luminescence in sulphide and silicate phosphors. Proc. Phys. Soc. Sect. A, Vol. 60: 574-590.*
3. *Van den Eeckhout, K., Smet, P. F., & Poelman, D. (2010), Persistent luminescence in Eu2+-doped compounds: a review. Materials, Vol. 3: 2536-2566.*
4. *Kamiya, S., & Mizuno, H. (1999). Phosphors for lamps, Second Edition, Phosphor Handbook.*
5. *Aitasalo, T.; Hölsä, J.; Laamanen, T., Lastusaari, M.; Lehto, L.; Niittykoski, J.; Pellé, F. (2005), Luminescence Properties of Eu2+ Doped Di barium Magnesium Di silicate, Ba2MgSi2O7:Eu2+. Ceramics – Silikáty, Vol. 49: 58-62.*
6. *Komeno, A.; Uemastu, K.; Toda, K.; Sato M. (2006), VUV properties of Eu-doped alkaline earth magnesium silicate. J. Alloys Compd. Vol. (408–412): 871–874.*
7. *Dubey SK, Sharma S, Diwakar AK, Pandey S. (2021), Synthesization of Monoclinic (Ba2MgSi2O7: Dy3+) Structure by Combustion Route. Journal of Materials Science Research and Reviews, Vol. 8: 172-179.*
8. *Sharma, S., & Dubey, S. K. (2021). The significant properties of silicate based luminescent nanomaterials in various fields of applications: a review. International Journal of Scientific Research in Physics and Applied Sciences, Vol. 9: 37-41.*
9. *Ekambaram, S., & Maaza, M. (2005), Combustion synthesis and luminescent properties of Eu3+-activated cheap red phosphors. Journal of alloys and compounds, Vol. 395: 132-134.*
10. *Kingsley JJ, Patil KC. (1988), A novel combustion process for the synthesis of fine particle α-alumina and related oxide materials. Materials letters, Vol. 6: 427-32.*
11. *JCPDS Pdf file number 23-0842, JCPDS International Center for Diffraction Data.*
12. *Aitasalo, T., Hölsä, J., Laamanen, T., Lastusaari, M., Lehto, L., Niittykoski, J., & Pellé, F. (2006), Crystal structure of the monoclinic Ba2MgSi2O7 persistent luminescence material. Zeitschrift fur Kristallographie Supplements, 481-486.*
13. *Sharma, S., Kumar Dubey, S., K Diwakar, A., & Pandey, S. (2021), Novel White Light Emitting (Ca2MgSi2O7: Dy3+) Phosphor. Journal of Material Science Research and Reviews, Article no. JMSRR 77178, Vol. 8: 164-171.*
14. *Jacob, R.; Isac, J. (2015), X ray diffraction line profile analysis of, international journal of chemical studies, Vol. 2: 12-21.*
15. *Warren, B. E., & Averbach, B. L. (1952), The separation of cold-work distortion and particle size broadening in X-ray patterns. Journal of applied physics, Vol. 23: 497.*
16. *Hall, W. H., & Williamson, G. K. (1951), The diffraction pattern of cold worked metals: I the nature of extinction. Proceedings of the Physical Society. Section B, Vol. 64: 937.*

17. *Wilson, A. J. C. (1987), Functional form of some ideal hypersymmetric distributions of structure factors. Acta Crystallographica Section A: Foundations of Crystallography, Vol. 43: 554-556.*

18. *Dubey, S. K., Sharma, S., Pandey, S., & Diwakar, A. K. (2021), Structural Characterization and Optical Properties of Monoclinic Ba2MgSi2O7 (BMS) Phosphor, IJSRPAS, Vol. 9: 81-85.*

19. *Sharma, S., Dubey, S. K.., (2022), Specific Role of Novel TL Material in Various Favorable Applications. Insights Min Sci technol., Vol. 3: 555609.*

20. *Dubey SK, Sharma S, Diwakar AK, (2021), Structural & thermal properties of monoclinic Ba2MgSi2O7 (BMS) Phosphor, Irjmets, Vol. 3: 677-682.*

21. *Chen, R., (1969), Glow curves with general order kinetics, Journal of the electrochemical society, Vol. 116: 1254.*

22. *Yuan, Z. X., Chang, C. K., Mao, D. L., & Ying, W., (2004), Effect of composition on the luminescent properties of Sr4Al14O25: Eu2+, Dy3+ phosphors, Journal of Alloys and Compounds, Vol. 377: 268-271.*

23. *McKeever, S. W. (1988). Thermoluminescence of solids, Third Edition, Cambridge University Press.*

24. *Mashangva, M., Singh, M.N. and Singh, T.B., (2011), Estimation of optimal trapping parameters relevant to persistent luminescence, Indian Journal of Pure & Applied Physics, Vol. 49: 583-589.*